Neural sensitization improves encoding fidelity in the primate retina

Todd R. Appleby[1,2,3] and Michael B. Manookin[2,3,*]

[1]Graduate Program in Neuroscience, University of Washington, Seattle, WA 98195, USA

[2]Department of Ophthalmology, University of Washington, Seattle, WA 98195, USA

[3]Vision Science Center, University of Washington, Seattle, WA 98195, USA

[*]Correspondence: manookin@uw.edu

ABSTRACT

Sensory neural circuits must create internal representations of the natural environment and update those representations when the environment changes. Many neurons perform these adjustments by adapting to the statistics of incoming stimuli, allowing these cells to then report when those statistics change. Other neural populations exhibit sensitization. Instead of aligning their input-output properties with stimulus statistics, the outputs of sensitizing cells closely track the variance of incoming stimuli. These forms of short-term plasticity are commonly thought to be opposing and complementary with adapting and sensitizing cells encoding strong and weak stimuli, respectively. We report that the numerically dominant output pathway in the macaque monkey retina, the midget (parvocellular-projecting) pathway, constitutes an exception to this rule. Midget cells strongly sensitize and lack a functional counterpart that displays adaptation. Instead of counterbalancing adapting cells, sensitization in midget cells supports accurate sensory encoding and prevents a loss of responsiveness during dynamic vision.

INTRODUCTION

The fundamental constraints on sensory coding require that neural circuits adjust their outputs based on the statistical properties of their recent inputs [1–3]. Neurons respond to dynamic inputs using two distinct strategies—adaptation and sensitization. Adapting cells respond to strong stimulation by decreasing their sensitivity and this decrease in responsiveness can persist for several seconds after the stimulus intensity decreases [3–9]. Thus, adapting cells are relatively insensitive to weak stimuli occurring during these transition periods. Sensitizing cells show the opposite pattern—increasing their responsiveness at these transitions [10–12]. For this reason, adaptation and sensitization are thought to constitute opposing and complementary forms of short-term neural plasticity [10,11].

This hypothesis requires that a sensitizing cell type have an adapting counterpart that encodes common information [10]. However, this constraint could potentially decrease the amount of information that can be encoded in an neural ensemble and increase the metabolic demands on a sensory tissue [3,13]. Alternatively, adaptation and sensitization could be signatures of fundamentally distinct neural coding strategies [14]. Further, these alternative hypotheses are not mutually exclusive—adapting and sensitizing cells could mirror each other in some species and neural pathways and not in others, depending on the particular coding and metabolic constraints in those systems [2,3,13,15]. However, given that neural sensitization was only recently discovered, relatively little is known about its roles in neural information processing.

To address this issue, we recorded from five types of output neurons in the macaque monkey retina—broad thorny (koniocellular-projecting), On and Off parasol (magnocellular-projecting), and On and Off midget (parvocellular-projecting) ganglion cells. These cells have well described roles in visual processing and no known functional counterparts. We studied how these cells responded to global fluctuations in contrast and other stimulus statistics. We report that whereas broad thorny and parasol cells strongly adapted, midget cells sensitized—increasing their responsiveness to certain types of visual stimulation, including high contrast and simulated eye movements. Synaptic current recordings revealed that this increased sensitivity was present in the excitatory input from midget bipolar cells and was mediated by presynaptic disinhibition. A computational model based on synaptic input recordings further indicated that this increase in sensitivity greatly enhanced the fidelity of encoding natural scenes. Moreover, the lack of an adapting counterpart to midget cells indicates that sensitizing circuits perform a distinct role in primate retina relative to that observed in other vertebrate neural systems [10–12,16].

RESULTS

The midget pathway of the primate retina is commonly believed to lack short-term plasticity mechanisms such as contrast gain control. This belief is based on reports that midget cells did not

exhibit noticeable changes in responsiveness following transitions from high to low contrast regimes [9,17]. The assay used to measure adaptation was a sinusoidally modulated drifting grating with bar widths tuned to the size of the midget cell receptive field center, which is narrower than many other retinal cell types. Thus, if plasticity in the midget pathway depended on mechanisms with broader spatial tuning, this assay would not engage such mechanisms.

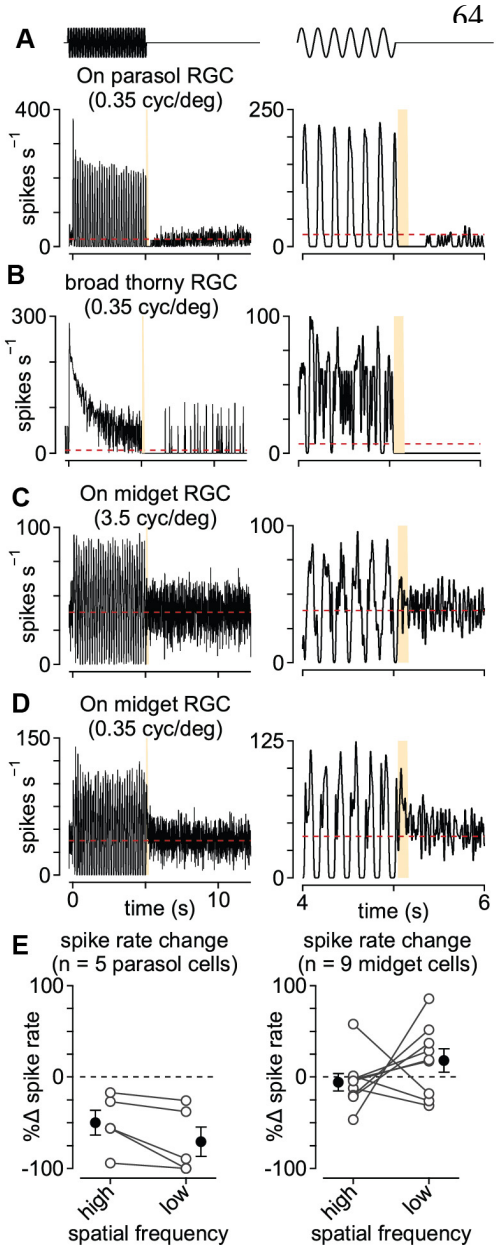

Figure 1. Parasol and midget cells exhibit opposing forms of plasticity.
(A) Spike rate in an On parasol ganglion cell to a low spatial frequency drifting grating presented for five seconds (temporal frequency, 6 Hz; spatial frequency, 0.35 cycles degree^{-1}). After the offset of high contrast, the spike rate declined below the level prior to grating onset (red dashed line). *Right*, zoom of transition period.
(B) Same as (A) in a broad thorny (On-Off type) ganglion cell.
(C) Same as (A) in an On midget ganglion cell to a high spatial frequency grating (3.5 cycles degree^{-1})
(D) Spike responses from the same cell as in (C) to a low spatial frequency grating (0.35 cycles degree^{-1}).
(E) Change in spike rate for the period directly after grating offset relative to period prior to grating onset in parasol (left) and midget ganglion cells (right).

To determine whether short-term plasticity in the midget pathway depended on the spatial properties of the stimulus, we repeated this assay while varying the spatial tuning of the gratings. At the offset of high contrast, midget cells did not exhibit a notable change in firing relative to the period that preceded high-contrast stimulation [9,17] (Figure 1C; spatial frequency, 3.5 cycles degree^{-1}). To determine whether this lack of either adaptation or sensitization persisted across a range of stimulus conditions, we varied the spatial frequency content of the drifting gratings. Following the offset of low spatial frequency gratings, most midget cells showed an increase in spiking relative to the period preceding grating onset (Figure 1D; spatial frequency, 0.35 cycles degree^{-1}). This increase in spiking following high contrast is characteristic of the contrast sensitization observed in other vertebrate retinas [10–12]. The presence

96 of sensitization at low spatial frequencies suggested that sensitization depended on the ability to
97 engage elements in the midget cell receptive field with broad spatial tuning relative to the midget
98 bipolar cell.
99
100 Parasol and broad thorny cells responded very differently than midgets. At the transition from high
101 to low contrast, these cells showed a pronounced decrease in spiking relative to the period before
102 the grating turned on and several seconds were required for the spike rate to recover (Figure 1A, B;
103 high contrast, 1.0; low contrast, 0.0; spatial frequency, 0.18-3.5 cycles degree^{-1}; grating size, 730 μm
104 × 730 μm). This behavior is characteristic of contrast adaptation—during periods of high contrast,
105 circuit mechanisms reduce the gain to avoid saturation and the gain remains low for several seconds
106 following the transition to a low-contrast regime [9,18,19].
107
108 **Wide-field stimulation evokes contrast sensitization in midget ganglion cells**
109 Our next goal was to determine how this putative wide-field component of the midget cell receptive
110 field contributed to contrast coding. To accomplish this goal, we sought a more spatially and
111 temporally precise assay of sensitivity following wide-field adaptation. Contrast tuning of parasol and
112 midget cells was determined with spots centered on the receptive field (duration, 0.1 s; parasol
113 diameter, 80-200 μm; midget diameter, 40-80 μm). Contrast responses were measured in isolation
114 (unadapted condition) or 50-100 msec following the offset of an adapting stimulus (adapted
115 condition). The adapting stimulus was a large, high-contrast spot modulated at 20-30 Hz (diameter,
116 730 μm; contrast, 0.5-1.0, duration, 1.25 s). Presentations of the adapted and unadapted stimuli were
117 interleaved to account for any potential variability in cellular responses over time.
118
119 Example spike responses to this stimulus paradigm are shown in Figure 2. Parasol cells increased
120 their spike rate at the onset of the adapting stimulus and the spike rate quickly decreased to a steady-
121 state rate by ~0.25 s. Test flashes presented after the offset of the adapting stimulus evoked fewer
122 spikes relative to the unadapted control (Figure 2A). Both of these patterns—a transient increase in
123 spike rate following the transition to high contrast and a decrease in spiking after the transition to
124 low contrast—are characteristic of cells undergoing contrast adaptation [4,6,20].
125
126 We modeled the variation in the contrast-response function following the adapting stimulus as a
127 change in the slope (gain) and a horizontal shift relative to the control condition (see Methods).
128 Following the adapting stimulus, parasol cells showed a large decrease in gain (–30.2 ± 4.5%; n = 5
129 cells; $p = 1.3 \times 10^{-3}$; Wilcoxon signed rank test, here and below) and a small rightward horizontal
130 shift (3.6 ± 1.5% contrast; $p = 3.0 \times 10^{-2}$) relative to the unadapted control (Figure 2C). This result
131 confirms previous reports that parasol cells readily adapt to contrast by continuously adjusting their
132 sensitivity to match the statistics of incoming visual inputs [9,17,18].

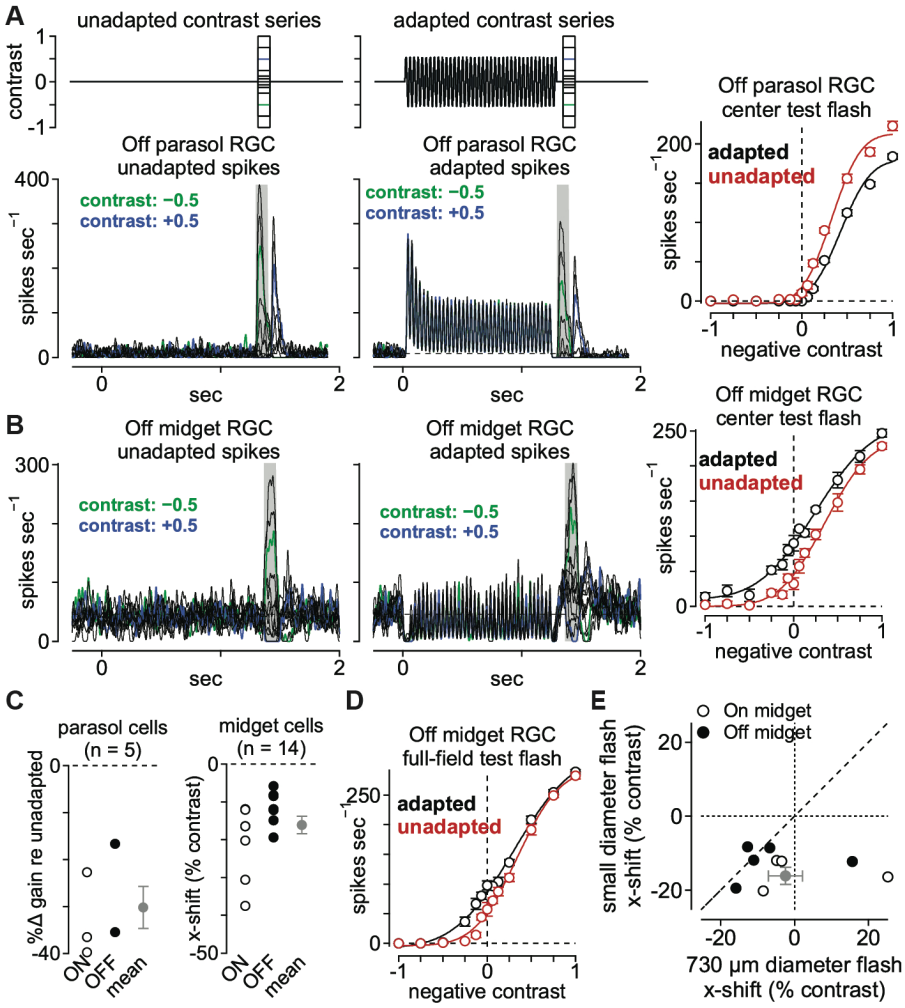

Figure 2. Midget ganglion cells display contrast sensitization.

(A) Spike responses from an Off parasol ganglion cell to a series of spots centered over the receptive-field. Spots were either presented alone (left) or 50 ms following the offset of an adapting stimulus (right). Shaded regions indicate sampling windows. *Right*, Average spike rate across the shaded regions. The wide-field adaptation evoked a decrease in the slope (gain) of the contrast-response curve (black) relative to the unadapted control condition (red).

(B) Same as (A) for an Off midget ganglion cell. *Right*, Average spike rate across the shaded regions. The wide-field adaptation evoked a leftward shift in the contrast-response curve (black) relative to the unadapted control condition (red).

(C) *Left*, Population data showing the change in slope (gain) for the adapted condition relative to the unadapted condition in On (open circles) and Off (closed circles) parasol ganglion cells (n = 5). *Right*, Population data showing the *x*-axis shift for adapted relative to unadapted conditions for small-diameter test flashes in On (open circles) and Off (closed circles) midget cells (n = 14). Gray circle and bars indicate mean ± SEM.

(D) Average spike rate evoked by wide-field test flashes for the Off midget cell in (B).

150 (E) Population data showing the *x*-axis shift for adapted relative to unadapted conditions for wide-
151 field test flashes versus small-diameter test flashes in On (open circles) and Off (closed circles)
152 midget cells. Gray circle and bars indicate mean ± SEM.
153
154 Midget cells showed several striking differences relative to the pattern observed in parasol cells.
155 First, the decrease in gain was much smaller in midget cells (–5.4 ± 4.3%; n = 14 cells; p = 0.12).
156 Second, an increase in spike rate was observed at the offset of the adapting stimulus relative to the
157 unadapted control (Figure 2B). This increase in spiking was evident at all contrasts tested including
158 the zero-contrast condition in which the spot intensity was equal to the average background
159 intensity. The elevation in spiking following the adapting stimulus produced a leftward shift in the
160 contrast-response curve relative to control (–16.2 ± 2.3% contrast; $p = 5.2 \times 10^{-6}$). A negative
161 horizontal shift value occurred when the adapted curve was shifted to the left of the control curve
162 and this indicated that a weaker stimulus was required to elicit the same spike response from a
163 midget cell following the adapting stimulus. This observation was consistent with previous reports
164 demonstrating that a decreased spike threshold, increased baseline response, and slight decrease in
165 gain are characteristic of contrast sensitization [10,11].
166
167 **Contrast sensitization is reduced for wide-field stimulation**
168 Midget cells show narrow receptive-field centers with strong input from the receptive-field surround
169 [21–23]. Thus, the effect of sensitization may be diminished following the adapting stimulus depending
170 on the relative influences of the direct midget bipolar cell input and wide-field mechanisms in
171 contrast sensitization. To determine whether contrast sensitization varied with the size of the test
172 flash, we repeated the adaptation experiment but used wide-field test flashes to measure the contrast
173 tuning of midget cells (diameter, 730 μm). The wide-field test flash evoked a slight leftward shift for
174 the adapted condition relative to control, but this shift was much smaller than was observed for the
175 small-diameter test flash in the same cell (compare Figure 2B, D). This trend held true across midget
176 cells—horizontal shifts were more negative for the small-diameter test flash than for the wide-field
177 test flash in the same cell and these shifts were not statistically significant for the wide-field test
178 flashes (x-shift, –2.4 ± 4.6% contrast; p = 0.30; gain change, –5.8 ± 5.8%; n = 9 cells; p = 0.17;
179 Figure 2E). These data indicated that the relative activations of narrow-field and wide-field
180 mechanisms during and following the adapting stimulus were critical to contrast sensitization in
181 midget ganglion cells. Moreover, this result agrees well with previous findings that did not report
182 contrast sensitization to wide-field noise [18].
183
184 **Time course for the onset and persistence of sensitization**
185 We next sought to determine the amount of stimulation needed to evoke sensitization and also how
186 long sensitization persisted after its onset. To determine the stimulation period needed to initiate

187 sensitization, we varied the presentation time of the adapting stimulus and measured the change in
188 spike rate relative to the unadapted control (adaptation duration, 0.25-1.25 sec; contrast, ±0.5;
189 duration, 0.1 sec). For each period of adaptation, midget cells showed an elevation in spiking relative
190 to unadapted controls (Figure 3A). Thus, sensitization could be elicited even with fairly brief
191 stimulus presentations.
192

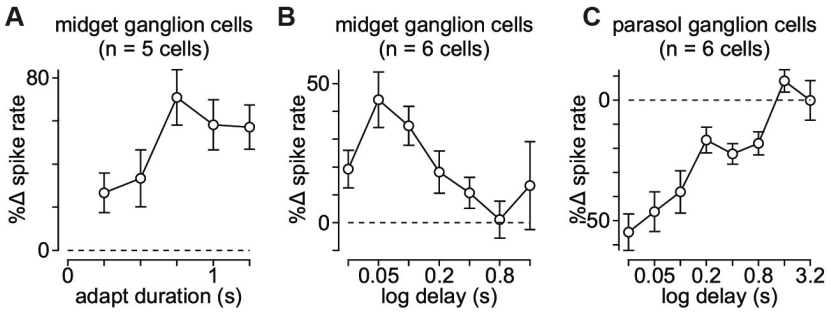

193
194 **Figure 3**. Time course of contrast sensitization and adaptation.
195 (A) Change in spike rate for the adapted condition relative to unadapted control for adaptation
196 periods (contrast, ±0.25-0.5; delay 0.05 s). Adaptation period was varied between 0.25-1.25 s (*x*-
197 axis).
198 (B) Duration of contrast sensitization in midget ganglion cells. Test flashes (contrast, ±0.25-0.5)
199 were presented at different delays (*x*-axis) following the offset of an adapting stimulus. Percent
200 change in spike rate for the adapted condition relative to the unadapted condition is shown on the *y*-
201 axis.
202 (C) Same as (B) for parasol ganglion cells.
203 Error bars indicate mean ± SEM.
204
205 To determine the time course of sensitization in midget cells, we measured spot responses at
206 different times following the offset of the adapting stimulus (delay, 0.025-1.6 sec; contrast, ±0.5;
207 duration, 0.1 sec). Relative to the unadapted control, the adapting stimulus elicited higher spike rates
208 to the test flash in midget cells at delays of 0.025-0.4 seconds (Figure 3B). This elevation in spiking,
209 characteristic of sensitization, was greatest 0.05-0.1 seconds after the offset of the adapting stimulus.
210 Parasol cells, on the other hand, showed a reduction in spiking to the same stimulus that persisted
211 for approximately one second (Figure 3C). Together, these data indicated that sensitization in midget
212 cells could be elicited even with fairly brief stimulus presentations and that it persisted for several
213 hundred milliseconds.
214
215 **Sensitization enhances chromatic processing in midget cells**
216 Midget ganglion cells in the central retina exhibit strong chromatic opponency which is formed from
217 differential input from long-wavelength cones (L cones) and middle-wavelength cones (M cones) to
218 the receptive-field center and surround [21–23]. To determine whether sensitization affected chromatic

219 processing, we measured contrast responses in midget cells with purely chromatic (isoluminant) test
220 flashes following the adapting stimulus.
221
222 Isoluminant (equiluminant) stimuli are commonly employed to study color mechanisms in isolation.
223 These stimuli are created by modulating L and M cones in opposing phases to silence achromatic
224 mechanisms that sum inputs from these cone types (i.e., L+M). We measured contrast-responses to
225 purely chromatic (isoluminant) flashes (duration, 0.1 sec) in the presence or absence of an
226 achromatic adapting stimulus, as above. As with the achromatic stimuli, the adapting stimulus
227 elicited a leftward shift to chromatic test contrasts (Figure 4). This shift was reminiscent of that
228 observed for achromatic stimulation (–11.3 ± 4.1% contrast; n = 8 cells; $p = 1.5 \times 10^{-2}$). These data
229 indicated that contrast sensitization enhanced both achromatic and chromatic processing in midget
230 cells.
231
232 While chromatic processing was affected by sensitization, the observation that an achromatic
233 adapting stimulus was sufficient to evoke sensitization indicated that chromatic circuits were not
234 necessary to elicit the phenomenon. These data did not, however, rule out contributions from purely
235 chromatic mechanisms to contrast sensitization.
236
237 **Sensitization does not arise from a chromatic mechanism**
238 To determine whether such a chromatic mechanism contributed to the observed contrast
239 sensitization, we presented a chromatic adapting stimulus. This stimulus was specifically designed to
240 modulate chromatic mechanisms that differentiate L- and M-cone inputs (L–M; isoluminant) while
241 silencing achromatic mechanisms that sum inputs from the L- and M-cone pathways (L+M;
242 isochromatic). Following the adapting stimulus, an isoluminant contrast series was used to measure
243 the input-output relationship. In the same cell, we compared chromatic contrast-responses following
244 a chromatic (L–M) or achromatic (L+M) adapting stimulus.
245
246 The achromatic adapting stimulus produced a leftward shift in the chromatic contrast-response
247 relation. The chromatic adapting stimulus, however, produced no such shift (x-shift, –1.1 ± 4.7%
248 contrast; n = 8 cells; p = 0.41). We interpreted this result as evidence that contrast sensitization
249 arose from an achromatic mechanism in the midget cell receptive-field. Moreover, given the role of
250 horizontal cells in forming the L-versus-M opponent receptive-field surround, these data excluded
251 horizontal cells as the source of sensitization in the midget pathway [21].

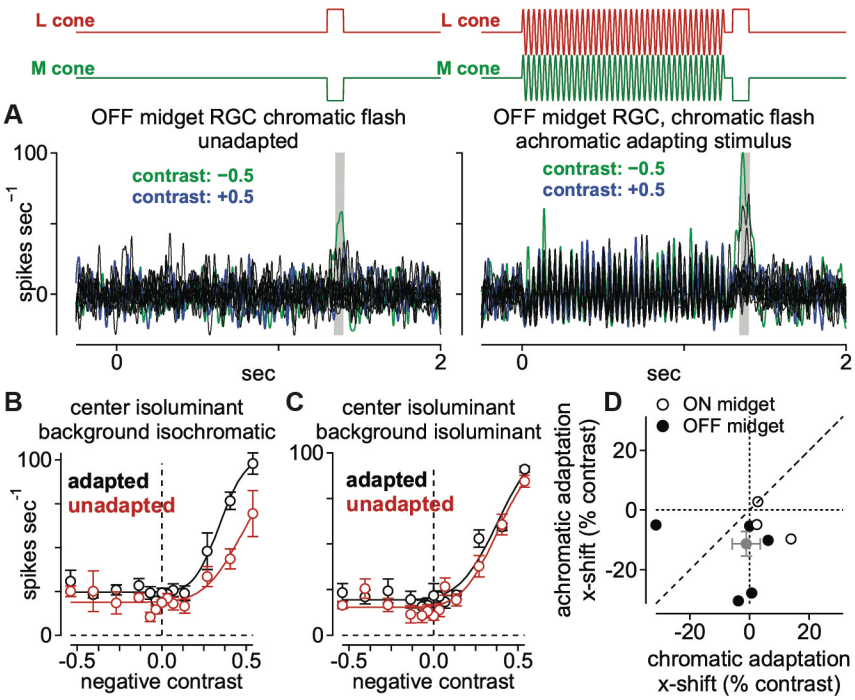

Figure 4. Sensitization arises from an achromatic mechanism.

(A) Spike responses from an Off midget ganglion cell to a chromatic (isoluminant) contrast series. Spots were either presented alone (left) or 50 msec following the offset of an achromatic adapting stimulus (right). Shaded regions indicate sampling windows.

(B) Average spike rate across the shaded regions indicated in (A). Achromatic adaptation evoked a leftward shift in the contrast-response curve (black) relative to the unadapted control condition (red) for the chromatic test flash.

(C) Same as (B) for a chromatic adapting stimulus. The chromatic adapting stimulus did not evoke change in the contrast-response curve relative to control.

(D) Population data showing the *x*-axis shift for adapted relative to unadapted conditions for a chromatic adapting stimulus (*x*-axis) relative to an achromatic adapting stimulus (*y*-axis) in On (open circles) and Off (closed circles) midget cells. Gray circle and bars indicate mean ± SEM.

Sensitization is present in excitatory synaptic input from midget bipolar cells

The experiments above found contrast sensitization in the spike output of midget ganglion cells. Our next goal was to understand the circuit mechanisms mediating sensitization. To accomplish this goal, we measured the direct excitatory and inhibitory synaptic inputs to midget ganglion cells with whole-cell, voltage-clamp recordings (see Methods). Excitatory currents were isolated by holding a cell's membrane voltage at the reversal potential for inhibition (–70 mV), and likewise, inhibitory currents were recorded at the excitatory reversal potential (0 mV). An increase in excitatory input to a cell was indicated by a more negative (inward) current relative to the leak current. Indeed, the adapting stimulus evoked larger inward excitatory currents relative to the unadapted control at all

contrasts tested (Figure 5A). Plotting excitatory charge as a function of contrast revealed a similar pattern to that observed in the spike recordings—the adapting stimulus evoked a leftward shift in the contrast-response curve relative to the unadapted control (Figure 5B). On average, the adapting stimulus elicited a horizontal shift of –11% contrast (–11.3 ± 4.2% contrast; n = 8 cells; $p = 1.95 \times 10^{-2}$). These results indicated that contrast sensitization was present in the excitatory synaptic input from midget bipolar cells to midget ganglion cells.

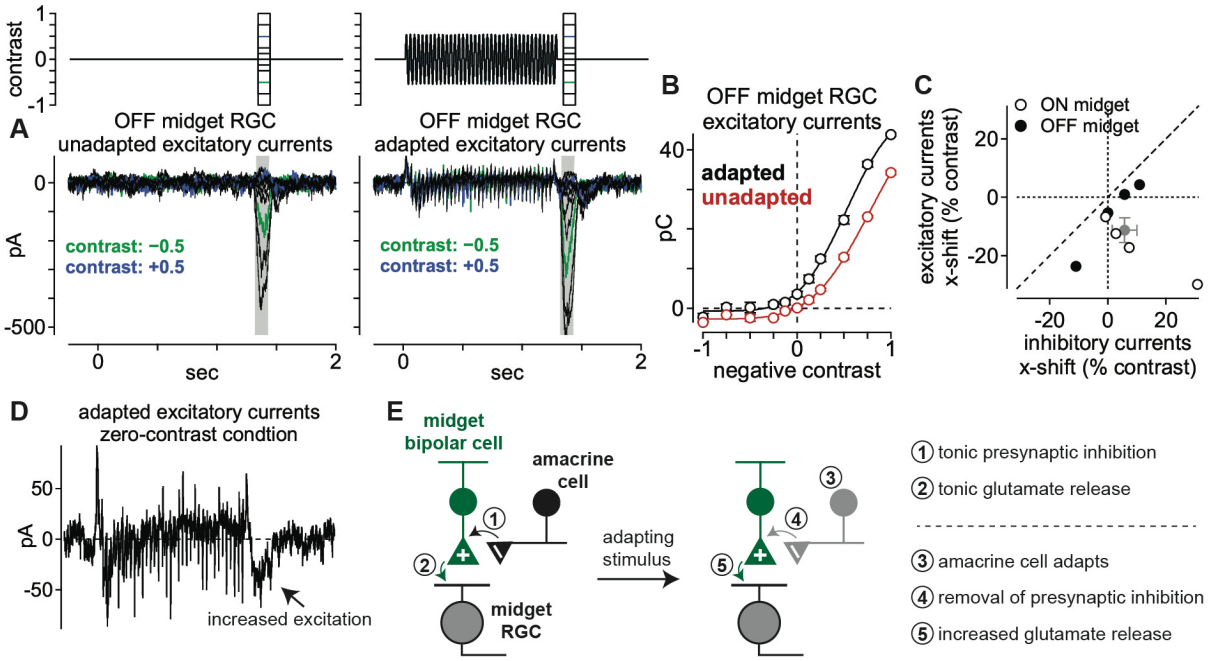

Figure 5. Sensitization present in excitatory synaptic input from midget bipolar cells.

(A) Excitatory currents from an Off midget ganglion cell to a series of spots (diameter, 40-80 µm) centered over the receptive field. Spots were either presented alone (*left*) or 50 msec following the offset of an adapting stimulus (*right*; diameter, 730 µm). Shaded regions indicate sampling windows.

(B) Average spike rate across the shaded regions indicated in (A). The wide-field adaptation evoked a leftward shift in the contrast-response curve (black) relative to the unadapted control condition (red).

(C) Population data showing the x-axis shift for adapted relative to unadapted conditions for excitatory versus inhibitory synaptic currents in On (open circles) and Off (closed circles) midget cells. Mean values are shown in gray. Error bars indicate mean ± SEM.

(D) Excitatory current recordings from the Off midget cell in (A) under the condition in which the stimulus intensity returned to the mean luminance after the offset of the adapting stimulus and an additional test flash was not presented (zero-contrast condition). A sustained increase in excitatory current was observed at the offset of that stimulus.

(E) Proposed model for contrast sensitization in midget bipolar cells.

299 We also tested for the presence of sensitization in the inhibitory synaptic inputs to midget cells.
300 Unlike the pattern observed in spiking and excitatory currents, the adapting stimulus did not
301 consistently elicit leftward shifts in the inhibitory contrast-response functions relative to control
302 (+5.8 ± 4.3% contrast; n = 8 cells; p = 0.25; Figure 5C). These data indicated that contrast
303 sensitization arose at or prior to the level of glutamate release from midget bipolar cells. This finding
304 was consistent with the circuit model for contrast sensitization in bipolar cells in the retinas of fish,
305 salamander, mice, and rabbits [10–12]. This model posited a mechanism in which a strongly adapting
306 amacrine cell drove sensitization by a mechanism of presynaptic inhibition at the bipolar cell
307 terminal [11]. During the adapting stimulus, the amacrine cell adapted such that it decreased release of
308 inhibitory neurotransmitter to the bipolar cell synaptic terminal relative to the tonic level following
309 stimulus offset. This presynaptic disinhibition, in turn, depolarized the bipolar cell synaptic terminal,
310 allowing the cell to utilize its full dynamic range in signaling via glutamate release to postsynaptic
311 ganglion cells.
312
313 Cleanly measuring the effects of presynaptic inhibition on circuit function has proven exceedingly
314 difficult as use of inhibitory receptor antagonists typically cause many off-target effects that make
315 data interpretation highly tenuous [24]. Indeed, adding inhibitory antagonists in primate retina evoked
316 significant increases in tonic glutamate release from bipolar cells and changed the contrast polarity of
317 On parasol cells [25]. Nonetheless, our spike and whole-cell recordings strongly supported the
318 proposed model in which contrast sensitization arose from disinhibition at the presynaptic bipolar
319 cell terminal [11]. First, the lack of sensitization to a purely chromatic (isoluminant) adapting stimulus
320 indicated that sensitization did not arise in the outer retina at the level of horizontal cell feedback
321 (Figure 4). Second, the effect of presynaptic disinhibition was seen in our excitatory current
322 recordings (Figure 5D). In one of our stimulus conditions the test flash contrast was zero such that
323 the stimulus intensity returned to the average background intensity at the offset of the adapting
324 stimulus. Although this stimulus lacked a change in contrast following the adapting stimulus, we
325 observed an increase in excitatory synaptic input (Figure 5D). This response pattern was consistent
326 with a decrease in presynaptic inhibition following the offset of the adapting stimulus, resulting in an
327 increase in glutamate release from midget bipolar cells. Thus, our recordings in midget pathway of
328 primate retina were consistent with the circuit motif proposed in other vertebrate species (Figure
329 5E; [11]).
330
331 **A contrast sensitization model reproduces midget cell responses**
332 Having established the presence of contrast sensitization in midget bipolar cells, we next sought to
333 understand the relevance of this neural computation to visual processing in primates. To accomplish
334 this goal, we developed a computational model of the proposed circuit in which bipolar cell
335 glutamate release was modulated through presynaptic amacrine cell inhibition [10–12]. Model

parameters were determined by recording excitatory and inhibitory synaptic current responses from midget ganglion cells to a Gaussian white noise stimulus (see Methods).

We modeled the midget bipolar and presynaptic amacrine cell pathways using the classical linear-nonlinear model with two modifications: 1) adaptation occurred at the amacrine cell output and 2) the amacrine cell output was applied to the bipolar cell model prior to the bipolar cell output nonlinearity (Figure 6A). The model parameters controlling presynaptic sensitization were fit from direct excitatory current recordings. In the same cell from which these parameters were determined, we measured excitatory current responses to the wide-field adapting stimulus (see Figure 5), and the model qualitatively reproduced the increase in excitatory currents following the offset of this adapting stimulus (Figure 6C).

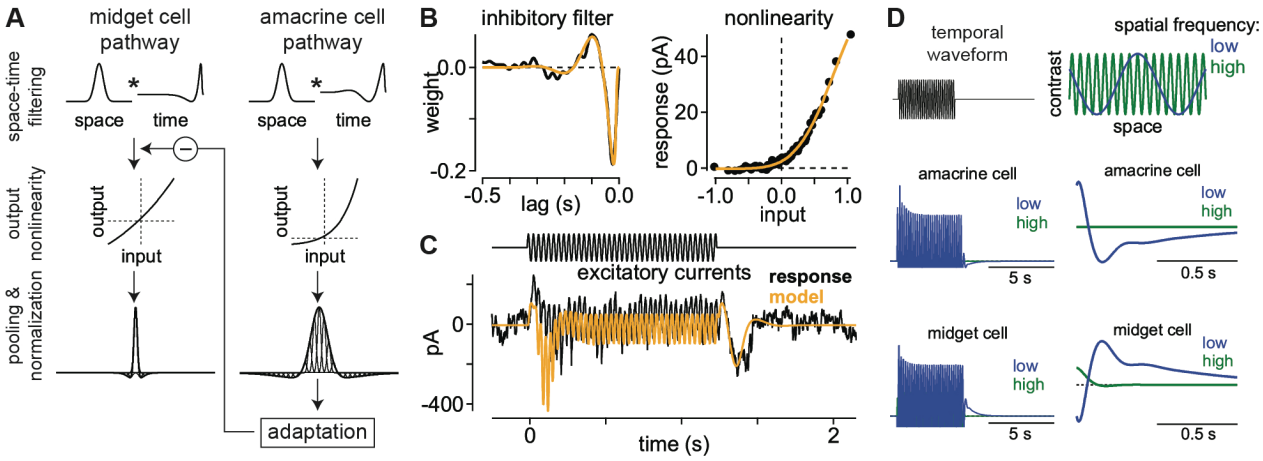

Figure 6. Sensitization model reproduces experimental results.

(A) Sensitization model structure. Visual inputs were convolved with a spatiotemporal linear filter comprised of a Gaussian in space and a biphasic filter in time. Signals in the amacrine cell pathway were then passed through an output nonlinearity before passing to the adaptation stage of the model. The output of the amacrine cell model provided inhibitory input to the midget bipolar cell pathway upstream of the bipolar cell output nonlinearity.

(B) Inhibitory temporal filter (*left*) and input-output nonlinearity (*right*) determined from noise recordings. These filters were then used as components of the computational model (A).

(C) Excitatory current recording from an Off midget ganglion cell to the wide-field adapting stimulus (see Figure 5). Model prediction (orange) was generated from excitatory synaptic current recordings to the noise stimulus in the same cell.

(D) Model output for drifting grating stimuli at high and low spatial frequencies.

We further tested the model using the drifting grating stimuli presented in Figure 1. The model produced distinct outputs for the high and low spatial frequency gratings. The high frequency grating produced a relatively small response and, as a result, little adaptation in the presynaptic

365 amacrine cell (Figure 6D, middle row). This was due to the broad receptive field center size of the
366 amacrine cell relative to the bars of the grating. Low frequency gratings, however, strongly
367 modulated the amacrine cell and produced significant adaptation; this adaptation, in turn, caused a
368 removal of inhibition at the level of the bipolar cell following the offset of the grating, resulting in
369 sensitization (Figure 6D, bottom row). The model predictions were qualitatively similar to our direct
370 recordings from midget cells, indicating that contrast sensitization in primate retina can be well
371 explained via presynaptic disinhibition as in other species [10–12].
372
373 **Sensitizing circuits more accurately reconstruct natural stimuli than adapting circuits**
374 We next sought to understand how these differing strategies of adaptation and sensitization
375 impacted encoding during naturalistic vision. This was done by testing the ability of adapting and
376 sensitizing models to accurately encode natural scenes. We specifically wanted to determine how
377 accurately downstream visual circuits could reconstruct naturalistic input stimuli based on the
378 outputs of populations of model On and Off midget ganglion cells. The naturalistic stimuli used in
379 the model were taken from the DOVES database—a dataset of eye movements in humans recorded
380 while observing natural images [26]. Reconstruction accuracy was determined by calculating the
381 correlation between the stimulus and response of each model (see Methods). Periods of fixation
382 between ballistic eye movements are critically important to visual coding in primates; thus, model
383 performance was separately calculated for the complete movie or for periods of fixation only.
384
385 We considered two different decoding models for estimating the stimulus contrast based on the
386 outputs of On and Off midget ganglion cells. The first model utilized a linear decoding scheme in
387 which stimulus contrast was estimated by taking the scaled difference between the On and Off cell
388 outputs. We also tested a quadratic decoding model that squared the On and Off outputs prior to
389 differencing (see Methods). Using these decoders, we compared the performance of the sensitization
390 model with a model in which the midget bipolar underwent contrast adaptation. Regardless of the
391 decoding scheme used, the sensitizing model showed higher accuracy for reconstructing the entire
392 stimulus trajectory than the adapting model (linear r^2: sensitization, 0.81 ± 0.05; adaptation, 0.23 ±
393 0.07; $p = 2.7 \times 10^{-54}$; quadratic r^2: sensitization, 0.84 ± 0.05; adaptation, 0.45 ± 0.09; $p = 2.9 \times 10^{-54}$;
394 n = 161 movies; mean ± SD; Figure 7C). The sensitizing model also outperformed the adapting
395 model when the analysis was restricted to periods of fixation (Figure 7D).
396
397 The sensitizing model showed increased encoding accuracy for periods of fixation relative to periods
398 of ballistic eye movements (movement r^2, 0.63 ± 0.12; $p = 2.9 \times 10^{-35}$; Figure 7E). This finding
399 suggested that sensitization could play a particularly important role in vision during periods of
400 fixation following the offset of global motion. We, thus, sought to determine whether background
401 motion could evoke contrast sensitization with direct recordings from midget ganglion cells.

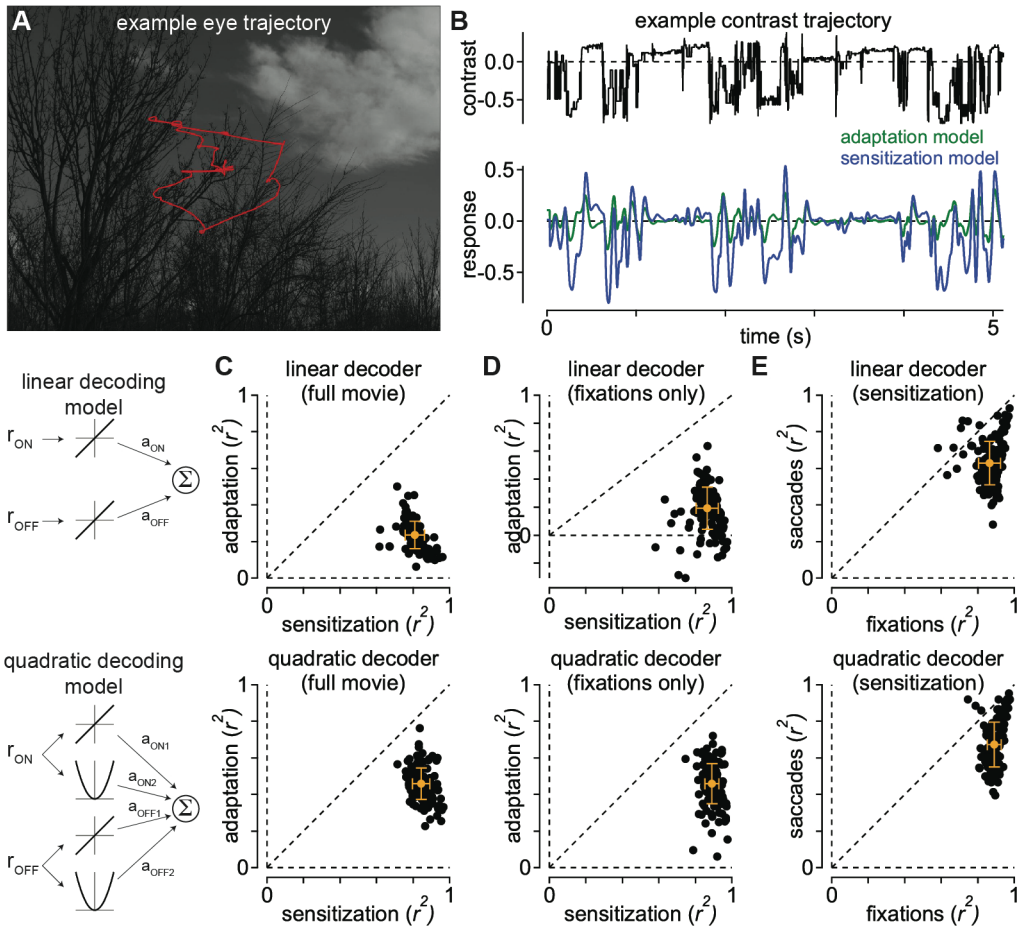

Figure 7. Sensitization increases the fidelity of encoding natural movies.

(A) Example image from the DOVES database. The observer's eye trajectory is shown in red.

(B) *Top*, temporal contrast sequence from the eye movement data in (A). *Bottom*, responses of the adaptation and sensitization models to the example contrast sequence.

(C) Performance of the sensitization (*x*-axis) and adaptation (*y*-axis) models at reconstructing 161 natural movies in the database. Performance was measured as the Pearson correlation between the stimulus and model predictions after adjusting for temporal lag. Performance for each movie is indicated by a black dot. Gray dot and bars indicate mean ± SD. The sensitization model outperformed the adaptation model for each of the movies.

(D) Model performances as in (C), but restricted to periods of fixation. The sensitization model outperformed the adaptation model in each case.

(E) Sensitization model performance for periods of fixation versus periods of eye motion. Predictive performance of the model was typically higher during periods of fixation.

Background motion evokes contrast sensitization in midget cells

To determine whether background motion elicited sensitization, we measured contrast responses in midget cells following the offset of a full-field moving texture (speed, 5-11 degrees s^{-1}; duration, 1 s).

The goal was to simulate, as closely as possible, the brief periods of fixation following eye movements and to test sensitivity during these fixation periods. We interleaved these recordings with measurements when the texture was stationary throughout the trial. The moving textures elicited an increase in spiking and a leftward shift in the contrast-response functions relative to the control condition in which the texture was stationary (Figure 8). On average, the shift was –25% contrast for spike recordings (–25.4 ± 4.4% contrast; n = 10 cells; $p = 2.4 \times 10^{-2}$) and –12% contrast for excitatory current recordings (–12.5 ± 5.1% contrast; n = 4 cells; $p = 2.4 \times 10^{-2}$).

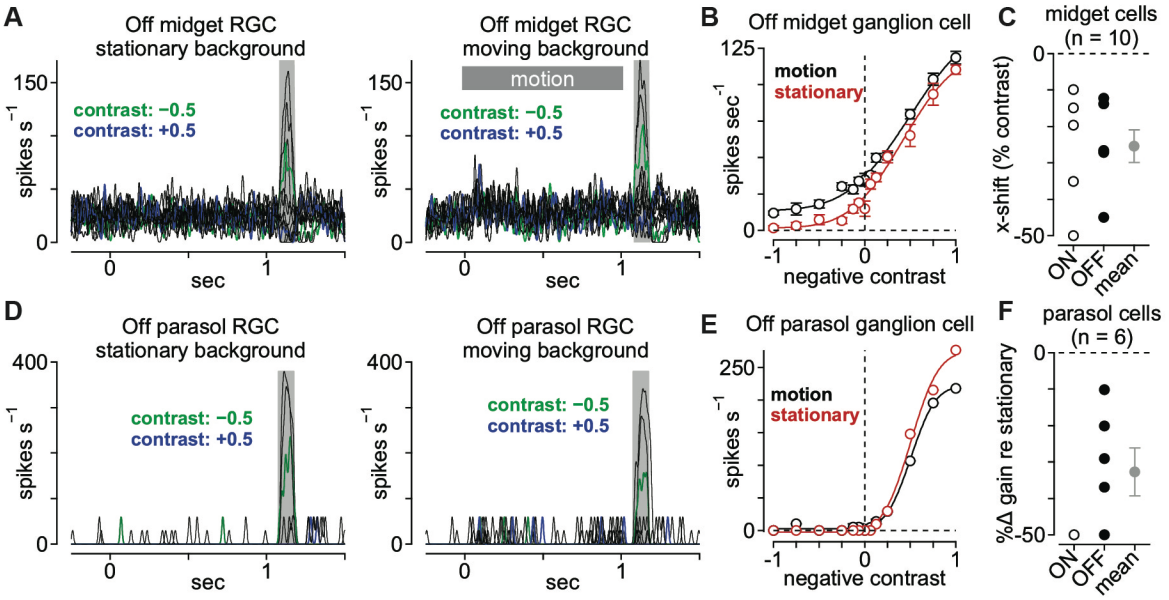

Figure 8. Background motion evokes contrast sensitization in midget cells.

(A) Spike responses from an Off midget ganglion cell to a series of spots centered over the receptive field. Spots were either presented alone (left) or 50 msec following the offset of background motion (speed, 11 degrees s^{-1}). Shaded regions indicate sampling windows.

(B) Average spike rate across the shaded regions indicated in (A). The wide-field adaptation evoked a leftward shift in the contrast-response curve (black) relative to the unadapted control condition (red).

(C) Horizontal shift (*x*-shift) in contrast-response function following background motion relative to control condition in which the background was stationary. Data are shown for On and Off midget ganglion cells (n = 10). Gray circle and bars indicate mean ± SEM.

(D) Same as (A) for an Off parasol ganglion cell.

(E) Same as (B) for the Off parasol cell in (D). The cell showed a decrease in spike output following the offset of background motion—the opposite pattern to that observed in the Off midget cell.

(F) Change in gain in the contrast-response function following background motion relative to the control condition. On average, background motion elicited a decrease in gain of ~30% relative to the control condition in which the background was stationary (n = 6 cells). Gray circle and bars indicate mean ± SEM.

These data were consistent with our circuit model of contrast sensitization. The amacrine cell providing presynaptic inhibition to the midget bipolar cell adapted during background motion; at the offset of motion, the cell hyperpolarized and reduced presynaptic inhibition to the bipolar terminal. Thus, similar to circuits described in other vertebrates, the midget pathway could utilize presynaptic inhibition to account for self-motion [11,27,28].

DISCUSSION

Our results support a novel role for neural sensitization in primates relative to the function proposed in other species. Sensitizing cells are commonly thought to counteract the loss of responsiveness experienced by adapting cells during transitions from high to low variance environments [10]. This hypothesis requires that sensitizing cells have an adapting counterpart that encodes similar information about the environment. Midget (parvocellular-projecting) ganglion cells are well known for their roles in both chromatic and achromatic vision [21–23]. Functional parallelism in the midget pathway is achieved by splitting signals between different classes of cone photoreceptor (L versus M) or bipolar cell (On versus Off) inputs to the midget cell receptive-field. Further, we found that both On- and Off-type midget cells exhibited sensitization (Figure 1-4, 8), and the primate retina lacks an adapting functional counterpart to midget cells with similar chromatic opponency or spatial acuity [29]; thus, sensitization does not counterbalance adaptation in another functionally parallel pathway.

Instead, our findings indicate that sensitization maintains the responsiveness of the midget pathway during dynamic visual processes, such as head or eye movements, that cause rapid fluctuations in light intensity on the retina. We base this conclusion on several key observations. First, sensitization was strongest following wide-field stimulation (Figure 1-4) or background motion (Figure 8). Second, sensitization persisted for >0.2 s (Figure 3), a period that roughly corresponds to the durations of fixations following eye movements in primates (reviewed in [30]). Finally, sensitization greatly improved the fidelity of encoding natural movies, particularly during periods of fixation following ballistic eye motion (Figure 7). Thus, sensitization appears to play a unique and crucial role in neural coding in primates.

Distinct functions of adaptation and sensitization in primate retina

Our findings also speak to the roles of neural adaptation in the parasol and broad thorny ganglion cell pathways. Previous work proposed that adapting cells could produce a nearly optimal faithful encoding of sensory inputs [31]. Our computational model, however, indicates that sensitizing circuits outperform adapting circuits in encoding natural movies (Figure 7). The improved reconstruction accuracy of the sensitizing model was consistent with a recent theoretical report indicating that

483 sensitizing cells are better for encoding faithful representations of sensory input than adapting cells
484 [14]. According to this paradigm, sensitizing cells such as midget ganglion cells would be useful for
485 directly encoding information about the properties of the input (e.g., contrast, color). Adapting cells,
486 on the other hand, are optimized for performing inference tasks [14,32].
487
488 Adapting cells dynamically adjust their input-output properties to align with the recent stimulus
489 distribution [4,8]. These adjustments make the cells exquisitely sensitive to changes in stimulus
490 statistics, allowing them to infer when salient properties of the environment change. For example,
491 quickly detecting object motion is an ethologically relevant and phylogenetically ancient neural
492 computation [33,34]; by decreasing their responsiveness during periods in which the background is
493 either stationary or coherently moving, adapting neural circuits would be poised to report when an
494 object moves relative to the background [27,35]. Interestingly, both adapting parasol and broad thorny
495 ganglion cells have been implicated in motion processing [25,35] and project to retinorecipient brain
496 regions in the lateral geniculate body, superior colliculus, and inferior pulvinar that contribute
497 significantly to motion vision [36–38].
498
499 **Relationship to psychophysical measurements in humans**
500 It has long been recognized that eye movements play important computational roles in visual
501 processing (reviewed in [39,40]). Periods in which an image is stabilized on the retina cause that image
502 to fade from perception [41] and small fixational eye movements appear to counteract this fading [42,43].
503 These eye movements can, however, produce large temporal fluctuations in contrast, particularly
504 when viewing high-contrast objects. This would, in turn, produce fading phenomena in cells that
505 strongly adapt, such as parasol ganglion cells—a prediction that was confirmed with our
506 computational model (Figure 7).
507
508 Neural mechanisms such as sensitization may serve to counteract adaptation by maintaining the
509 sensitivity of certain visual pathways during eye movements. Indeed, our computational model and
510 direct measurements indicated that contrast sensitization in the midget ganglion cell pathway was
511 engaged well by background motion such as that observed during eye movements (Figure 7, 8).
512 Thus, contrast sensitization might act to maintain sensitivity of image-forming visual pathways
513 following eye movements that are commonplace in primate vision. Indeed, psychophysical studies in
514 humans indicated that contrast sensitivity increases following both ballistic (saccade) and fixational
515 eye movements [42,43]. Moreover, this increase in sensitivity was limited to chromatic stimuli and high-
516 spatial-frequency achromatic stimuli, mirroring our results in midget ganglion cells.
517

518 **METHODS**

519 Experiments were performed in an *in vitro*, pigment-epithelium attached preparation of the macaque
520 monkey retina [44]. Eyes were dissected from terminally anesthetized macaque monkeys of either sex
521 (Macaca *fascicularis*, *mulatta*, and *nemestrina*) obtained through the Tissue Distribution Program of the
522 National Primate Research Center at the University of Washington. All procedures were approved
523 by the University of Washington Institutional Animal Care and Use Committee.

524

525 **Tissue Preparation and Electrophysiology**

526 The retina was continuously superfused with warmed (32-35°C) Ames' medium (Sigma) at ~6-8 mL
527 min^{-1}. Recordings were performed from macular, mid-peripheral, or peripheral retina (2-8 mm, 10-
528 30° foveal eccentricity), but special emphasis was placed on recording from more centrally located
529 cells. Physiological data were acquired at 10 kHz using a Multiclamp 700B amplifier (Molecular
530 Devices), Bessel filtered at 3 kHz (900 CT, Frequency Devices), digitized using an ITC-18 analog-
531 digital board (HEKA Instruments), and acquired using the Symphony acquisition software package
532 developed in Fred Rieke's laboratory (http://symphony-das.github.io).

533

534 Recordings were performed using borosilicate glass pipettes containing Ames medium for
535 extracellular spike recording or, for whole-cell recording, a cesium-based internal solution containing
536 (in mM): 105 $CsCH_3SO_3$, 10 TEA-Cl, 20 HEPES, 10 EGTA, 2 QX-314, 5 Mg-ATP, and 0.5 Tris-
537 GTP, pH ~7.3 with CsOH, ~280 mOsm. Series resistance (~3-9 MΩ) was compensated online by
538 50%. The membrane potential was corrected offline for the approximately –11 mV liquid junction
539 potential between the intracellular solution and the extracellular medium. Excitatory and inhibitory
540 synaptic currents were isolated by holding midget ganglion cells at the reversal potentials for
541 inhibition/chloride (~–70 mV) and excitation (0 mV), respectively.

542

543 **Visual Stimuli and Data Analysis**

544 Visual stimuli were generated using the Stage software package developed in the Rieke lab
545 (http://stage-vss.github.io) and displayed on a digital light projector (Lightcrafter 4500; Texas
546 Instruments) modified with custom LEDs with peak wavelengths of 405, 505 (or 475), and 640 nm.
547 Stimuli were focused on the photoreceptor outer segments through a 10X microscope objective.
548 Mean light levels were in the low to medium photopic regimes (~3×10^3 – 3.4×10^4
549 photoisomerizations [R*] $cone^{-1}$ sec^{-1}). Contrast values for contrast-response flashes are given in
550 Weber contrast and for periodic stimuli in Michaelson contrast. All responses were analyzed in
551 MATLAB (R2018a+, Mathworks).

552

553 For extracellular recordings, currents were wavelet filtered to remove slow drift and amplify spikes
554 relative to the noise [45] and spikes were detected using either a custom k-means clustering algorithm

or by choosing a manual threshold. Whole-cell recordings were leak subtracted and responses were measured relative to the median membrane currents immediately preceding stimulus onset (0.25-0.5 s window). Summary data are presented in terms of conductance (g), which is the ratio of the current response (I) to the driving force:

$$g = \frac{I}{V_m - E}$$

where V_m is the holding potential (in mV) and E is the reversal potential (in mV). Reversal potentials of 0 mV and –70 mV were used for excitatory and inhibitory inputs, respectively.

Sensitization and adaptation models

We modeled spatiotemporal integration in bipolar cells and amacrine cells as the product of a Gaussian spatial filter and a biphasic temporal filter which was then passed through an input-output nonlinearity. The output of this nonlinear stage of the amacrine cell model was then passed through an adaptation stage; adaptation in the amacrine cell provided inhibitory input to the bipolar cell model prior to the output nonlinearity (Figure 6A). Following the subunit output, model midget ganglion cells and amacrine cells pooled (summed) inputs from bipolar cell subunits and the weights of these inputs were normalized by the subunit location relative to the receptive field center using a Gaussian weighting.

To estimate the excitatory and inhibitory circuit components for the computational model, we recorded excitatory and inhibitory synaptic currents from midget ganglion cells in response to a full-field Gaussian flicker stimulus. The contrast of each frame was drawn randomly from a Gaussian distribution and that value was multiplied by the average contrast. Average contrast was updated every 0.5 s and drawn from a uniform distribution (0.05-0.35 RMS contrast). The linear temporal filters (F) were calculated by cross-correlating the stimulus sequence (S) and the leak-subtracted response (R) [4].

$$F(t) = \int R(\tau)S(t+\tau)d\tau$$

where τ is the temporal lag. These filters were then modeled as a damped oscillator with an S-shaped onset [46,47]:

$$F(t) = A\frac{(t/\tau_{rise})^n}{1+(t/\tau_{rise})^n}e^{-\left(\frac{t}{\tau_{decay}}\right)}cos\left(\frac{2\pi t}{\tau_{period}}+\varphi\right)$$

where A is a scaling factor, τ_{rise} is the rising-phase time constant, τ_{decay} is the damping time constant, τ_{period} is the oscillator period, and φ is the phase (in degrees).

The input-output nonlinearity was calculated by convolving the temporal filter (F) and stimulus (S) to generate the linear prediction (P).

$$P(t) = \int F(\tau)S(t-\tau)d\tau$$

The prediction (*x*-axis) and response (*y*-axis) were modeled as a cumulative Gaussian distribution [48].

$$N(x) = \varepsilon + \frac{\alpha}{\sqrt{2\pi}} \int_{-\infty}^{x} e^{\frac{-(\beta t+\gamma)^2}{2}} dt$$

where a indicates the maximal output value, ε is the vertical offset, β is the sensitivity of the output to the generator signal (input), and γ is the maintained input to the cell.

The spatial component of the bipolar and amacrine cell receptive fields was modeled as a Gaussian function with a 2-SD width of 18 μm and 90 μm, respectively. Each midget ganglion cell was modeled as receiving input from a single bipolar cell, as is typically the case in the central retina. Sensitization parameters were determined by fitting linear-nonlinear model predictions relative to the excitatory currents recorded to the Gaussian flicker stimulus.

The amacrine cell providing direct inhibition to the midget ganglion cells is likely distinct from the cell providing presynaptic inhibition at the level of the midget bipolar cell (see Figure 5). Thus, our inhibitory synaptic recordings likely did not grant us direct access to the properties of the amacrine cell responsible for contrast sensitization. These recordings do, however, provide an estimate of the time-course of signals passing through the presynaptic amacrine cell to midget bipolar cells. Signals passing through this amacrine cell proceed from cone photoreceptors to bipolar cells and then to the amacrine cell in question before providing input to the midget bipolar cell. In the same way, the amacrine cell providing direct inhibition to midget ganglion cells must pass through an extra synapse. Thus, our recordings of direct synaptic inhibition were useful in approximating the time course of presynaptic inhibition at the midget bipolar terminal.

Evaluating model performance to naturalistic movies

We evaluated the performance of the adaptation and sensitization models in reconstructing the naturalistic movie sequences using linear and quadratic decoding paradigms. To estimate stimulus contrast, the linear decoder (f_{LINEAR}) summed the scaled outputs of the model On and Off midget ganglion cells:

$$f_{\text{LINEAR}}(t) = a_{\text{ON}} r_{\text{ON}}(t) + a_{\text{OFF}} r_{\text{OFF}}(t) + k$$

where a_{ON} and a_{OFF} are scaling constants and k is an offset constant. The quadratic model was similar in structure except that the response from each pathways was squared prior to summation:

$$f_{\text{QUADRATIC}}(t) = a_{\text{ON1}} r_{\text{ON}}(t) + a_{\text{ON2}} r_{\text{ON}}^2(t) + a_{\text{OFF1}} r_{\text{OFF}}(t) + a_{\text{OFF2}} r_{\text{OFF}}^2(t) + k$$

For each of the 161 movies in the database, the input stimulus was shifted to the peak of the midget temporal filter (~35 ms) and then scaling and offset coefficients were determined using least-squares curve fitting. The Pearson correlation was then calculated between the temporal trajectories of the model and the movie.

625

626 **Quantification and Statistical Analysis**

627 All statistical analyses were performed in MATLAB (R2018a+, Mathworks). Reported p values in
628 this study were paired and were calculated using the Wilcoxon signed-rank test. Final figures were
629 created in MATLAB, Igor Pro, and Adobe Illustrator.

630

631 **ACKNOWLEDGEMENTS**

632 We thank Shellee Cunnington, Mark Cafaro, and Jim Kuchenbecker for technical assistance. Tissue
633 was provided by the Tissue Distribution Program at the Washington National Primate Research
634 Center (WaNPRC; supported through NIH grant P51 OD-010425), and we thank the WaNPRC
635 staff, particularly Chris English, for making these experiments possible. Fred Rieke, Raunak Sinha,
636 Max Turner, and Will Grimes assisted in tissue preparation. We thank Jay Neitz and Fred Rieke for
637 helpful discussions. We also thank Alison Weber and Jon Demb for feedback on a previous version
638 of this manuscript. This work was supported in part by grants from the NIH (NEI R01-EY027323
639 to M.B.M.; NEI P30-EY001730 to the Vision Core), Research to Prevent Blindness Unrestricted
640 Grant (to the University of Washington Department of Ophthalmology), Latham Vision Research
641 Innovation Award (to M.B.M.), and the Alcon Young Investigator Award (to M.B.M.).

642

643 **AUTHOR CONTRIBUTIONS**

644 Conceptualization, M.B.M.; Methodology, M.B.M.; Software, M.B.M.; Formal Analysis, M.B.M.;
645 Investigation, M.B.M., T.R.A; Resources, M.B.M.; Data Curation, M.B.M., T.R.A.; Writing –
646 Original Draft, M.B.M.; Writing – Review & Editing, M.B.M., T.R.A.; Visualization, M.B.M.;
647 Supervision, M.B.M.; Project Administration, M.B.M.; Funding Acquisition, M.B.M. The ORCID
648 number for M.B.M. is 0000-0001-8116-7619.

649

650 **COMPETING INTERESTS**

651 The authors declare no competing interests.

652

653

654 **REFERENCES**

655 1. Srinivasan, M. V., Laughlin, S. B. & Dubs, A. Predictive coding: a fresh view of inhibition in the retina.
656 *Proc. R. Soc. Lond. B Biol. Sci.* **216,** 427–459 (1982).
657 2. Barlow, H. B. The coding of sensory messages. in *Current problems in animal behaviour* (eds. Thorpe, W. H.
658 & Zangwill, O. L.) 331–360 (Cambridge University Press, 1961).
659 3. Laughlin, S. A simple coding procedure enhances a neuron's information capacity. *Z. Naturforsch. C* **36,**
660 910–912 (1981).
661 4. Baccus, S. A. & Meister, M. Fast and slow contrast adaptation in retinal circuitry. *Neuron* **36,** 909–919
662 (2002).
663 5. Carandini, M. & Ferster, D. A tonic hyperpolarization underlying contrast adaptation in cat visual
664 cortex. *Science* **276,** 949–952 (1997).
665 6. Kim, K. J. & Rieke, F. Temporal contrast adaptation in the input and output signals of salamander
666 retinal ganglion cells. *J. Neurosci.* **21,** 287–299 (2001).
667 7. Manookin, M. B. & Demb, J. B. Presynaptic mechanism for slow contrast adaptation in mammalian
668 retinal ganglion cells. *Neuron* **50,** 453–464 (2006).
669 8. Smirnakis, S. M., Berry, M. J., Warland, D. K., Bialek, W. & Meister, M. Adaptation of retinal processing
670 to image contrast and spatial scale. *Nature* **386,** 69–73 (1997).
671 9. Solomon, S. G., Peirce, J. W., Dhruv, N. T. & Lennie, P. Profound contrast adaptation early in the visual
672 pathway. *Neuron* **42,** 155–162 (2004).
673 10. Kastner, D. B. & Baccus, S. A. Coordinated dynamic encoding in the retina using opposing forms of
674 plasticity. *Nat. Neurosci.* **14,** 1317–1322 (2011).
675 11. Kastner, D. B. & Baccus, S. A. Spatial segregation of adaptation and predictive sensitization in retinal
676 ganglion cells. *Neuron* **79,** 541–554 (2013).
677 12. Nikolaev, A., Leung, K. M., Odermatt, B. & Lagnado, L. Synaptic mechanisms of adaptation and
678 sensitization in the retina. *Nat. Neurosci.* **16,** 934–941 (2013).
679 13. Balasubramanian, V., Kimber, D. & Berry, M. J., 2nd. Metabolically efficient information processing.
680 *Neural Comput.* **13,** 799–815 (2001).

681 14. Mlynarski, W. F. & Hermundstad, A. M. Adaptive coding for dynamic sensory inference. *Elife* **7,** (2018).
682 15. Levy, W. B. & Baxter, R. A. Energy efficient neural codes. *Neural Comput.* **8,** 531–543 (1996).
683 16. Cohen-Kashi Malina, K., Jubran, M., Katz, Y. & Lampl, I. Imbalance between excitation and inhibition
684 in the somatosensory cortex produces postadaptation facilitation. *J. Neurosci.* **33,** 8463–8471 (2013).
685 17. Benardete, E. A., Kaplan, E. & Knight, B. W. Contrast gain control in the primate retina: P cells are not
686 X-like, some M cells are. *Vis. Neurosci.* **8,** 483–486 (1992).
687 18. Chander, D. & Chichilnisky, E. J. Adaptation to temporal contrast in primate and salamander retina. *J.*
688 *Neurosci.* **21,** 9904–9916 (2001).
689 19. Benardete, E. A. & Kaplan, E. The dynamics of primate M retinal ganglion cells. *Vis. Neurosci.* **16,** 355–
690 368 (1999).
691 20. Brown, S. P. & Masland, R. H. Spatial scale and cellular substrate of contrast adaptation by retinal
692 ganglion cells. *Nat. Neurosci.* **4,** 44–51 (2001).
693 21. Crook, J. D., Manookin, M. B., Packer, O. S. & Dacey, D. M. Horizontal cell feedback without cone
694 type-selective inhibition mediates 'red-green' color opponency in midget ganglion cells of the primate
695 retina. *J. Neurosci.* **31,** 1762–1772 (2011).
696 22. De Monasterio, F. M. & Gouras, P. Functional properties of ganglion cells of the rhesus monkey retina.
697 *J. Physiol.* **251,** 167–195 (1975).
698 23. Derrington, A. M., Krauskopf, J. & Lennie, P. Chromatic mechanisms in lateral geniculate nucleus of
699 macaque. *J. Physiol.* **357,** 241–265 (1984).
700 24. Cook, P. B., Lukasiewicz, P. D. & McReynolds, J. S. Action potentials are required for the lateral
701 transmission of glycinergic transient inhibition in the amphibian retina. *J. Neurosci.* **18,** 2301–2308 (1998).
702 25. Manookin, M. B., Patterson, S. S. & Linehan, C. M. Neural Mechanisms Mediating Motion Sensitivity in
703 Parasol Ganglion Cells of the Primate Retina. *Neuron* **97,** 1327–1340.e4 (2018).
704 26. Van Der Linde, I., Rajashekar, U., Bovik, A. C. & Cormack, L. K. DOVES: a database of visual eye
705 movements. *Spat. Vis.* **22,** 161–177 (2009).
706 27. Olveczky, B. P., Baccus, S. A. & Meister, M. Segregation of object and background motion in the retina.
707 *Nature* **423,** 401–408 (2003).
708 28. Baccus, S. A., Ölveczky, B. P., Manu, M. & Meister, M. A retinal circuit that computes object motion. *J.*

709 *Neurosci.* **28,** 6807–6817 (2008).

710 29. Wässle, H. Parallel processing in the mammalian retina. *Nat. Rev. Neurosci.* **5,** 747–757 (2004).

711 30. Rayner, K. Eye movements in reading and information processing: 20 years of research. *Psychol. Bull.*
712 **124,** 372–422 (1998).

713 31. Fairhall, A. L., Lewen, G. D., Bialek, W. & de Ruyter Van Steveninck, R. R. Efficiency and ambiguity in
714 an adaptive neural code. *Nature* **412,** 787–792 (2001).

715 32. Wark, B., Fairhall, A. & Rieke, F. Timescales of inference in visual adaptation. *Neuron* **61,** 750–761
716 (2009).

717 33. Frost, B. J., Wylie, D. R. & Wang, Y. C. The processing of object and self-motion in the tectofugal and
718 accessory optic pathways of birds. *Vision Res.* **30,** 1677–1688 (1990).

719 34. Lettvin, J. Y., Maturana, H. R., McCulloch, W. S. & Pitts, W. H. What the Frog's Eye Tells the Frog's
720 Brain. *Proceedings of the IRE* **47,** 1940–1951 (1959).

721 35. Puller, C., Manookin, M. B., Neitz, J., Rieke, F. & Neitz, M. Broad thorny ganglion cells: a candidate for
722 visual pursuit error signaling in the primate retina. *J. Neurosci.* **35,** 5397–5408 (2015).

723 36. Rodieck, R. W. & Watanabe, M. Survey of the morphology of macaque retinal ganglion cells that project
724 to the pretectum, superior colliculus, and parvicellular laminae of the lateral geniculate nucleus. *J. Comp.*
725 *Neurol.* **338,** 289–303 (1993).

726 37. Crook, J. D. *et al.* Y-cell receptive field and collicular projection of parasol ganglion cells in macaque
727 monkey retina. *J. Neurosci.* **28,** 11277–11291 (2008).

728 38. Kwan, W. C. *et al.* Unravelling the subcortical and retinal circuitry of the primate inferior pulvinar. *J.*
729 *Comp. Neurol.* (2018). doi:10.1002/cne.24387

730 39. Martinez-Conde, S., Macknik, S. L. & Hubel, D. H. The role of fixational eye movements in visual
731 perception. *Nat. Rev. Neurosci.* **5,** 229–240 (2004).

732 40. Rucci, M. & Victor, J. D. The unsteady eye: an information-processing stage, not a bug. *Trends Neurosci.*
733 **38,** 195–206 (2015).

734 41. Troxler, D. Verschwinden gegebener Gegenstände innerhalb unseres Gesichtskreises. *Ophthalmologische*
735 *Bibliothek* **2,** 1–53 (1804).

736 42. Rucci, M., Iovin, R., Poletti, M. & Santini, F. Miniature eye movements enhance fine spatial detail.

737 *Nature* **447,** 851–854 (2007).

738 43. Schütz, A. C., Braun, D. I., Kerzel, D. & Gegenfurtner, K. R. Improved visual sensitivity during smooth
739 pursuit eye movements. *Nat. Neurosci.* **11,** 1211–1216 (2008).

740 44. Manookin, M. B., Puller, C., Rieke, F., Neitz, J. & Neitz, M. Distinctive receptive field and physiological
741 properties of a wide-field amacrine cell in the macaque monkey retina. *J. Neurophysiol.* **114,** 1606–1616
742 (2015).

743 45. Wiltschko, A. B., Gage, G. J. & Berke, J. D. Wavelet filtering before spike detection preserves waveform
744 shape and enhances single-unit discrimination. *J. Neurosci. Methods* **173,** 34–40 (2008).

745 46. Schnapf, J. L., Nunn, B. J., Meister, M. & Baylor, D. A. Visual transduction in cones of the monkey
746 Macaca fascicularis. *J. Physiol.* **427,** 681–713 (1990).

747 47. Angueyra, J. M. & Rieke, F. Origin and effect of phototransduction noise in primate cone
748 photoreceptors. *Nat. Neurosci.* **16,** 1692–1700 (2013).

749 48. Chichilnisky, E. J. A simple white noise analysis of neuronal light responses. *Network* **12,** 199–213 (2001).

750
751

752 **FIGURE LEGENDS**

753

754 **Figure 1**. Parasol and midget cells exhibit opposing forms of plasticity.

755 (A) Spike rate in an On parasol ganglion cell to a low spatial frequency drifting grating presented for
756 five seconds (temporal frequency, 6 Hz; spatial frequency, 0.35 cycles degree^{-1}). After the offset of
757 high contrast, the spike rate declined below the level prior to grating onset (red dashed line). *Right*,
758 zoom of transition period.

759 (B) Same as (A) in a broad thorny (On-Off type) ganglion cell.

760 (C) Same as (A) in an On midget ganglion cell to a high spatial frequency grating (3.5 cycles degree^{-1})

761 (D) Spike responses from the same cell as in (C) to a low spatial frequency grating (0.35 cycles
762 degree^{-1}).

763 (E) Change in spike rate for the period directly after grating offset relative to period prior to grating
764 onset in parasol (left) and midget ganglion cells (right).

765

766 **Figure 2**. Midget ganglion cells display contrast sensitization.

767 (A) Spike responses from an Off parasol ganglion cell to a series of spots centered over the
768 receptive-field. Spots were either presented alone (left) or 50 ms following the offset of an adapting
769 stimulus (right). Shaded regions indicate sampling windows. *Right*, Average spike rate across the
770 shaded regions. The wide-field adaptation evoked a decrease in the slope (gain) of the contrast-
771 response curve (black) relative to the unadapted control condition (red).

772 (B) Same as (A) for an Off midget ganglion cell. *Right*, Average spike rate across the shaded regions.
773 The wide-field adaptation evoked a leftward shift in the contrast-response curve (black) relative to
774 the unadapted control condition (red).

775 (C) *Left*, Population data showing the change in slope (gain) for the adapted condition relative to the
776 unadapted condition in On (open circles) and Off (closed circles) parasol ganglion cells (n = 5).
777 *Right*, Population data showing the *x*-axis shift for adapted relative to unadapted conditions for
778 small-diameter test flashes in On (open circles) and Off (closed circles) midget cells (n = 14). Gray
779 circle and bars indicate mean ± SEM.

780 (D) Average spike rate evoked by wide-field test flashes for the Off midget cell in (B).

781 (E) Population data showing the *x*-axis shift for adapted relative to unadapted conditions for wide-
782 field test flashes versus small-diameter test flashes in On (open circles) and Off (closed circles)
783 midget cells. Gray circle and bars indicate mean ± SEM.

784

785

786

787

788

Figure 3. Time course of contrast sensitization and adaptation.
(A) Change in spike rate for the adapted condition relative to unadapted control for adaptation periods (contrast, ±0.25-0.5; delay 0.05 s). Adaptation period was varied between 0.25-1.25 s (*x*-axis).
(B) Duration of contrast sensitization in midget ganglion cells. Test flashes (contrast, ±0.25-0.5) were presented at different delays (*x*-axis) following the offset of an adapting stimulus. Percent change in spike rate for the adapted condition relative to the unadapted condition is shown on the *y*-axis.
(C) Same as (B) for parasol ganglion cells.
Error bars indicate mean ± SEM.

Figure 4. Sensitization arises from an achromatic mechanism.
(A) Spike responses from an Off midget ganglion cell to a chromatic (isoluminant) contrast series. Spots were either presented alone (left) or 50 msec following the offset of an achromatic adapting stimulus (right). Shaded regions indicate sampling windows.
(B) Average spike rate across the shaded regions indicated in (A). Achromatic adaptation evoked a leftward shift in the contrast-response curve (black) relative to the unadapted control condition (red) for the chromatic test flash.
(C) Same as (B) for a chromatic adapting stimulus. The chromatic adapting stimulus did not evoke change in the contrast-response curve relative to control.
(D) Population data showing the *x*-axis shift for adapted relative to unadapted conditions for a chromatic adapting stimulus (*x*-axis) relative to an achromatic adapting stimulus (*y*-axis) in On (open circles) and Off (closed circles) midget cells. Gray circle and bars indicate mean ± SEM.

826 **Figure 5**. Sensitization present in excitatory synaptic input from midget bipolar cells.
827 (A) Excitatory currents from an Off midget ganglion cell to a series of spots (diameter, 40-80 μm)
828 centered over the receptive field. Spots were either presented alone (*left*) or 50 msec following the
829 offset of an adapting stimulus (*right*; diameter, 730 μm). Shaded regions indicate sampling windows.
830 (B) Average spike rate across the shaded regions indicated in (A). The wide-field adaptation evoked
831 a leftward shift in the contrast-response curve (black) relative to the unadapted control condition
832 (red).
833 (C) Population data showing the x-axis shift for adapted relative to unadapted conditions for
834 excitatory versus inhibitory synaptic currents in On (open circles) and Off (closed circles) midget
835 cells. Mean values are shown in gray. Error bars indicate mean ± SEM.
836 (D) Excitatory current recordings from the Off midget cell in (A) under the condition in which the
837 stimulus intensity returned to the mean luminance after the offset of the adapting stimulus and an
838 additional test flash was not presented (zero-contrast condition). A sustained increase in excitatory
839 current was observed at the offset of that stimulus.
840 (E) Proposed model for contrast sensitization in midget bipolar cells.
841
842 **Figure 6**. Sensitization model reproduces experimental results.
843 (A) Sensitization model structure. Visual inputs were convolved with a spatiotemporal linear filter
844 comprised of a Gaussian in space and a biphasic filter in time. Signals in the amacrine cell pathway
845 were then passed through an output nonlinearity before passing to the adaptation stage of the
846 model. The output of the amacrine cell model provided inhibitory input to the midget bipolar cell
847 pathway upstream of the bipolar cell output nonlinearity.
848 (B) Inhibitory temporal filter (*left*) and input-output nonlinearity (*right*) determined from noise
849 recordings. These filters were then used as components of the computational model (A).
850 (C) Excitatory current recording from an Off midget ganglion cell to the wide-field adapting
851 stimulus (see Figure 5). Model prediction (orange) was generated from excitatory synaptic current
852 recordings to the noise stimulus in the same cell.
853
854
855
856
857
858
859
860
861
862

863 **Figure 7**. Sensitization increases fidelity of encoding natural movies.
864 (A) Example image from the DOVES database. The observer's eye trajectory is shown in red.
865 (B) *Top*, temporal contrast sequence from the eye movement data in (A). *Bottom*, responses of the
866 adaptation and sensitization models to the example contrast sequence.
867 (C) Performance of the sensitization (*x*-axis) and adaptation (*y*-axis) models at reconstructing 161
868 natural movies in the database. Performance was measured as the Pearson correlation between the
869 stimulus and model predictions after adjusting for temporal lag. Performance for each movie is
870 indicated by a black dot. Gray dot and bars indicate mean ± SD. The sensitization model
871 outperformed the adaptation model for each of the movies.
872 (D) Model performances as in (C), but restricted to periods of fixation. The sensitization model
873 outperformed the adaptation model in each case.
874 (E) Sensitization model performance for periods of fixation versus periods of eye motion. Predictive
875 performance of the model was typically higher during periods of fixation.
876
877 **Figure 8**. Background motion evokes contrast sensitization in midget cells.
878 (A) Spike responses from an Off midget ganglion cell to a series of spots centered over the receptive
879 field. Spots were either presented alone (left) or 50 msec following the offset of background motion
880 (speed, 11 degrees s^{-1}). Shaded regions indicate sampling windows.
881 (B) Average spike rate across the shaded regions indicated in (A). The wide-field adaptation evoked
882 a leftward shift in the contrast-response curve (black) relative to the unadapted control condition
883 (red).
884 (C) Horizontal shift (*x*-shift) in contrast-response function following background motion relative to
885 control condition in which the background was stationary. Data are shown for On and Off midget
886 ganglion cells (n = 10). Gray circle and bars indicate mean ± SEM.
887 (D) Same as (A) for an Off parasol ganglion cell.
888 (E) Same as (B) for the Off parasol cell in (D). The cell showed a decrease in spike output following
889 the offset of background motion—the opposite pattern to that observed in the Off midget cell.
890 (F) Change in gain in the contrast-response function following background motion relative to the
891 control condition. On average, background motion elicited a decrease in gain of ~30% relative to
892 the control condition in which the background was stationary (n = 6 cells). Gray circle and bars
893 indicate mean ± SEM.